Optical Engineering

SPIEDigitalLibrary.org/oe

Design, development, and in-flight testing of a pointer/tracker for in-flight experiments to measure aero-optical effects over a scaled turret

Matthew J. Krizo
Salvatore J. Cusumano
Steven T. Fiorino
Ryan Heap
Victor Velten
Joshua Brown
Richard J. Bartell

SPIE

Design, development, and in-flight testing of a pointer/tracker for in-flight experiments to measure aero-optical effects over a scaled turret

Matthew J. Krizo
Salvatore J. Cusumano
Steven T. Fiorino
Ryan Heap
Victor Velten
Joshua Brown
Richard J. Bartell
Air Force Institute of Technology
Center for Directed Energy
Department of Engineering Physics
2950 Hobson Way
Wright-Patterson AFB, Ohio 45433
E-mail: matthew.krizo@afit.edu

Abstract. We address the design, development, and testing of a pointer/tracker as a probe beam for the purpose of making high-speed, aero-optical measurements of the flow over a scaled beam director turret. The tracker uses retro-reflection of the probe beam off of a Reflexite annulus surrounding the turret. The constraints of the design required a near-total-commercial off the shelf system that could be quickly installed and removed in a rented aircraft. Baseline measurements of environmental vibrations are used to predict pointing performance; mitigation of line-of-sight jitter on the probe beam is achieved through passive isolation and the design of relay optics. Accommodation of ambient light is made with the use of wavelength filters and track algorithms. Postanalysis of measured data is compared to design estimates. [DOI: 10.1117/1.OE.52.7.071415]

Subject terms: real-time; tracking; centroid; Airborne Aero-Optics Laboratory.

Paper 121583SS received Oct. 31, 2012; revised manuscript received Jan. 10, 2013; accepted for publication Feb. 6, 2013; published online Apr. 9, 2013.

1 Introduction

Aero-optics can be a significant degrader of the coherence of a high-energy laser (HEL) beam as it exits from a beam director on an airborne platform. Early research on this effect recognized its deleterious effects, but the first HELs, being at the much longer wavelength of 10.6 μm, were not degraded significantly by the pressure and temperature changes of the flow over the exit window of the beam director turret. The current status of solid state lasers makes them viable sources for tactical scenarios because of weight-to-power ratios and the brightness of the source. While these devices have typical wavelengths around 1 μm, the exact wavelength is not considered important in this study because the expected degradation due to aero-optical flow will be severe regardless of the choice of wavelength, if not mitigated or corrected.[1–3]

The High Energy Laser—Joint Technology Office (HEL-JTO) recognized the need to better understand these phenomena, and funded the Airborne Aero-Optics Laboratory (AAOL) multidisciplinary research initiative. The AAOL initiative seeks to reverse this shortfall by adding a flight test as a viable and affordable experimental tool to not only advance the scientific foundations for aero-optic effects, but explore mitigation schemes involving flow control and adaptive optics. Such a bold undertaking requires a team with an in-depth understanding of the underlying physics, computational fluid dynamics (CFD), modeling, experimental methods, and flight operations; the AAOL participants comprise such a team. The AAOL team includes a partnering between the University of Notre Dame, the Air Force Institute of Technology (AFIT), MZA Associates, and Boeing SVS.

The flight-test component is the unique aspect of this program; however, the success in building the AAOL and, as importantly, the interpretation of the data collected in flight heavily depends on the coordinated use of computations, modeling, and wind-tunnel testing. As such, the AAOL is a coordinated program that links advanced CFD to wind-tunnel testing, and wind-tunnel testing to a flight test. The need to include CFD, modeling, simulation, and wind-tunnel testing in the development of the flight platform brings together recognized experts in their respective fields as a team that will build scientific knowledge even as the design of the flight laboratory and test scenarios develop.

The flight-test laboratory consists of a main data-acquisition aircraft (the AAOL itself), with an integrated turret complemented by a laser source aircraft that will fly in relatively close formation with the AAOL; both aircrafts will be able to achieve transonic flight. The laser source plane will point a diverging, initially small-diameter laser beam onto the turret pupil on the AAOL. The rationale for the use of the small beam at the source was that the beam would be small compared to the coherence length of the optically relevant turbulent structures inside a thin turbulent boundary layer present on the skin of the laser aircraft;[4] the beam's small diameter would then only allow the boundary-layer turbulence on the source aircraft to impose slight tip-tilt on the beam. Once the beam is received at the turret on the AAOL it is stabilized and directed onto the optical bench where a suite of instruments will measure the incoming wavefronts at both high-temporal and spatial bandwidths. This paper focuses on the development the AFIT active pointer/tracker (AAPT) system, which is the diverging laser source required for these measurements.

2 Background

The AAPT system is installed on the laser source aircraft and provides the previously mentioned small initial diameter diverging beam that is required for wavefront measurements. In addition, the AAPT system must track the aperture on the turret of the AAOL aircraft to ensure that the laser light is received by the AAOL aircraft.

2.1 *AAPT Hardware Design*

The design of the AAPT system is heavily influenced by the space available in the aircraft, but it must also meet the design requirements. The highest level design requirements are listed in Table 1. The development of these requirements is further explored by Jumper et al.,[5] also found in this issue.

From these requirements, some initial decisions could be made. From requirements 2 and 3, we concluded that we would use a 5W 532-nm Spectra Physics Millennia laser. This could be designed to provide the 2× overfill in diameter space (requirement 3), as long as overall optical transmission remains greater than 0.8 while simultaneously delivering 1W into the input pupil (requirement 2). The divergence of the beam required to create the appropriate spot size will also produce the illumination and phase simulating a point source (requirement 2). The Spectra Physics laser has a beam quality of $M^2 = 1.1$. This is a very high beam quality for a laser of this wavelength and power level. The beam quality (requirement 4) will be retained if all optics are chosen with good wavefront error (WFE) specifications.

The location of system install has a profound impact on requirements 1, 5, 6, 7, and 8. There are two major options that were considered. The first was to install the beam director in the forward baggage compartment. This is an unpressurized, unconditioned compartment in the nose of the plane. This location was considered because the curvature of the nose of the plane afforded excellent view forward. This location allows for the AAOL turret to be looking backward which is (requirement 6) a region of particular interest for an aero-optic study. Additionally, it would be relatively easy to obtain a replacement and modify this door so that the modified door would be used as part of the flight test operations. The other location considered was to use the main passenger cabin and use a window in the aircraft as an exit for the laser. The passenger compartment requires no special environmental design because the aircraft is pressurized and temperature controlled.

Ultimately, we chose to mount the equipment in the main cabin. We ruled out the forward baggage compartment for a number of reasons. The main reason is that the Millenia laser must operate in a controlled temperature and pressure. This would require a fiber optic, which would route through a pressure bulkhead, to bring the light from the source to the beam director in the forward compartment. To maintain beam quality, a single mode fiber is required. Single-mode fibers have a much smaller diameter, so maintaining the power transmission and beam quality would require an extremely precise, free-space fiber coupling. This type of setup would be highly susceptible to misalignment power loss from vibration. Adjustment of this coupling in flight would not be possible.

Table 1 Design requirements.

Requirement number	Description
1	Minimize beam jitter to less than 1 mrad
2	Deliver 1 W laser energy at 532 nm into 10.18 cm pupil with spherical wavefront at 50 m
3	Overfill input pupil by factor of two
4	Laser beam should have beam quality approaching $M^2 = 1$
5	Work at altitudes up to 40 kft
6	Maximize field of regard (FOR)
7	Minimize install impact into rented aircraft
8	No major modifications to aircraft

After the decision was made to use the main cabin as the location for the system, the first step was to model the destination aircraft. The system must then be able to direct the diverging laser beam over a large field of regard using only minor modifications to the aircraft. The small diameter of the exiting beam helps to minimize the turbulence developed on the skin of the laser source aircraft. The short (50-m) path reduces the impact of atmospheric turbulence.

There were two possible system designs considered for the main cabin. One main consideration was to determine what modifications to the aircraft were acceptable to the owners. The only potentially feasible modification would be to obtain a second cabin door to modify for the experiment. The modified door would be swapped for the original whenever the plane was converted for flight testing.

We analyzed two specific modifications to the main door. The first was to mount a bubble window that would house a small fiber-fed turret. This would give tremendous field of regard due to the laser source's position outside of the aircraft skin, but was of course limited by the same fiber coupling issues that partially eliminated the use of the forward baggage compartment.

We then considered adding a larger bubble dome to the door to accommodate a coude path type turret. A coude path turret injects the laser through a series of fold mirrors that sit on the azimuth and elevation rotation axes. This allows the system to have a superior field of view, but it involves a more complicated design. No COTS systems exist, so this type of design was eliminated for cost and schedule reasons.

The last modification would be to enlarge the flat window in the main crew door. The original Plexiglas window is slightly curved to match the aircraft body shape, but it is soft and often scratched. We analyzed the use of a larger, flat, high-quality BK6 glass window. The larger size helps improve the field of regard, (requirement 6), and improves beam quality (requirement 4). In the end, we found that the glass window would be feasible, although the stress from the differential pressure at 25 + kft made the safety margin uncomfortably small. This window would require careful, regular inspection. However, the cost of a replacement door and the labor to change out the main door (~24 man hours per change) proved to be too costly. The decision was made to use the existing Plexiglas window on the usual cabin door.

2.2 *Field of Regard Analysis*

Use of the aircraft window led us to use a heliostat design. This is a two-axis (azimuth and elevation), flat mirror used to steer the beam. The limitations of using a heliostat mirror and flat window on the field of regard led us to the decision that we need to vary the location of the heliostat mirror with

respect to the aircraft window. This essentially is same technique of moving one's head naturally when looking out a flat window. Moving one's head to one side extends their outside view in the opposite direction. We chose to allow for three positions forward, centered, and aft. These positions maximize view angles for the extreme forward, extreme aft, and centered in the window for the best coverage for a single position. These positions are combined with two vertical positions that maximize the view up or down for a total of six possible positions.

Figure 1 illustrates the composite field of regard (FOR) of all six positions. The azimuth on the plot corresponds to turret azimuth and elevation of the AAOL turret. The regions in red are excluded by obstructions. The cause of the obstructions is labeled. The green region is shows the areas that can be achieved using the flat window design. The areas of darker green are in the overlap of more than one of the six positions. The region in white is the space that could be used if the AAPT were capable of the full 2-pi steradian field of view. We feel that the green area meets requirement 6 because it contains many points of scientific interest yet meets cost and schedule constraints. To enlarge the FOR, a much larger flat or domed window would be required. As it was previously discussed, changing the window on the aircraft was a time-consuming operation. To meet requirements 7 and 8, we will use the existing plexiglas window.

2.3 *Hardware Design*

Key hardware components in the final design include a Millenia Pro 5W 532-nm laser, an Aerotech 2-axis gimbal with a 100-mm diameter tip/tilt mirror, a 50-mm diameter Optics In Motion OIM102 fast steering mirror (FSM), high speed visible/near infrared AVT Marlin F131B, National Instruments PXI Real-Time system, and a desktop computer for user control.

The optical path through the system is as follows. The light from the laser passes through a computer-controlled shutter for safety. This allows for automatic shutdown in the event of a tracking failure. Following the shutter, the beam is expanded by 3× in diameter. This expansion reduces the intensity on the coated aluminum-fold mirrors. Without the beam expansion, laser intensity is about 90% of the rated intensity for the mirrors. Then a 600-mm-focal-length negative lens causes the light to diverge at the appropriate rate.

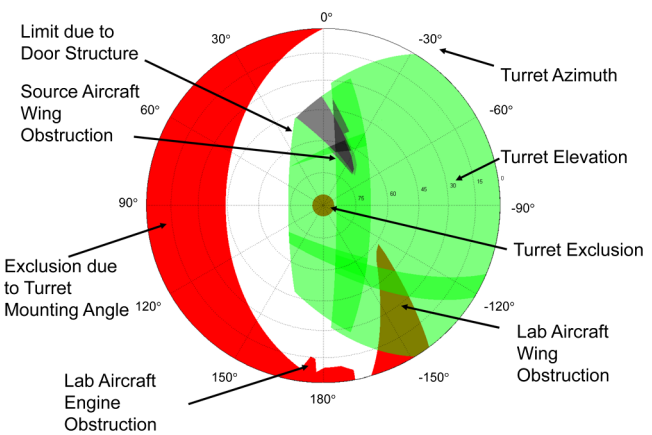

Fig. 1 Field of regard summary.

A mirror with a hole in its center is used to align the laser axis with the tracking system. The laser is propagated through the hole in the mirror, and the camera uses the rest of the mirror to have the same line of sight. The camera is set to a long focal length so the hole in the mirror does not show in the camera imagery. Last, the laser and the camera field of view encounter the fast steering mirror and the Aerotech heliostat.

Figure 2 shows the beam origin of the final system installed in the airplane. Figure 3 shows the beam steering components of the final system. Not pictured is the camera, as that is located underneath the OIM102 FSM. The system provides robust tracking and the desired factor of 2 overfill of the AAOL aperture at a working distance of 50 m. The system was completed and tested at the University of Notre Dame in August 2009.

To better visualize the installation into the aircraft, Fig. 4 shows the SolidWorks™ rendering of the final hardware design installed in the aircraft. It clearly shows the equipment racks on the left side of the figure. The larger table (edge

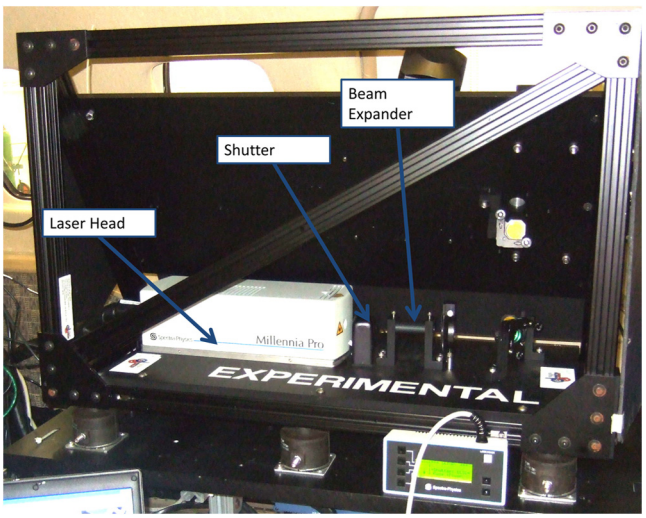

Fig. 2 Tracker assembly beam origin.

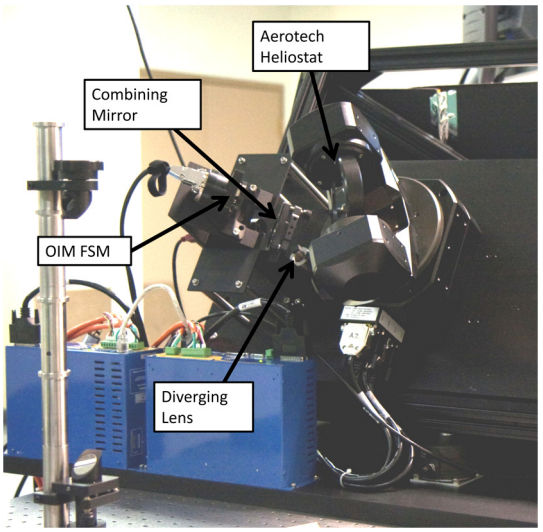

Fig. 3 View of beam directing optics.

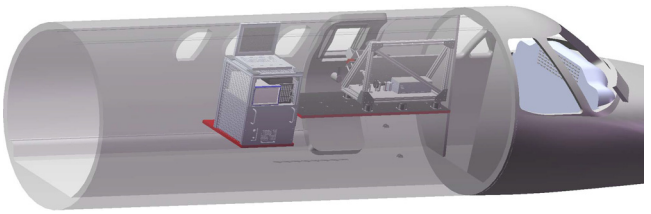

Fig. 4 SolidWorks rendering of the Air Force Institute of Technology active pointer/tracker (AAPT) installation.

colored red) centered in front of the door allows the AAPT system to be adjusted to maximize forward or rear FOR. The slanted plate nearest the wall of the aircraft is also able to slide on the triangle frame to maximize upward and downward FOR. These adjustments allow the system to be adjusted to provide a large FOR with no impact on the airflow around the laser source aircraft.

3 Tracker Capabilities

In track mode, we want the fastest possible tracking with the selected hardware. The main limiting factors are the camera running at 900 fps and the track algorithm, which must be able to run at this rate. Our selected hardware is only capable of completing a relatively simple track algorithm at that speed. We selected centroid tracking. This algorithm is the simplest computationally, and should work very well with the strong return signals from the retro-reflective (Reflexite™) tape. This will provide the accuracy we need and the ability to run at high frame rates.

3.1 *Centroid Tracker*

A centroid tracker is a term that applies to many types of trackers that employ a weighted sum over a subset of image pixels. Equation (1) below shows the characteristic equation for finding the y centroid in a continuous and discrete case. The methodology of finding the subset and weight of the pixels is how each tracker varies. All centroid-based trackers have one common thread: they all use some threshold value to initially find the subset of pixel to employ. From this, either the whole subset is used or a fraction of pixels leading in the direction of motion are used. AFIT/CDE had a selection of centroid algorithms available from Simulated Airborne Laser version 4.17b5, specifically energy, leading edge, polynomial edge, and n-row leading-edge centroid algorithms. The energy-based centroid (uses whole set of threshold pixels) was used since the other centroid algorithms need information about the direction of motion of the object, and thus, energy centroiding requires less user input.

$$y_c = \frac{\int\int y \cdot w(x,y)\mathrm{d}x\mathrm{d}y}{\int\int w(x,y)\mathrm{d}x\mathrm{d}y} = \frac{\sum_{i,j} i \cdot w(i,j)}{\sum_{i,j} w(i,j)}. \quad (1)$$

For the energy-based centroid, there are three different types of weighting functions: binary, type I, and type II weighting. Binary is the basic operation where weights are given a value of one or zero based on if they meet the threshold. Type I is where pixels who do not meet the threshold are set to zero and type II is similar to type I, except the pixel values are scaled down by the threshold. The major advantage of type II is that quantization effects are minimized. However, without quantization effects, type I has the best performance under noise, and binary is best where glints or other bright aberrations are present. The AAPT allows the user to choose between binary and type 1 thresholding. Both have been used successfully in flight.

Centroid-based tracking is good when there is a clear intensity difference between the target and background. Centroid trackers have been shown to be optimal in a least squares sense when the target has a parabolic intensity distribution.[6] Additionally, centroid trackers are very fast and have a small computational load. However, centroid trackers do suffer under scenarios where the target and background have low contrast. This limitation has been observed when the laser encounters the aircraft window at a shallow angle. A large amount of light is reflected back into the camera, which can exceed the return from the Reflexite tape.

Additionally, flying glints of sunlight reflected off the AAOL plane create a big problem with loss of contrast. The approach taken to dealing with sunlight was to recognize the broadband nature of sunlight compared to the narrow-line width of our laser. We placed a 10-nm full width half max (FWHM) bandpass filter, centered at 532 nm, in front of the camera. We found this reduced the intensity of the sunlight by a factor of 30. After the addition of this filter, the system could track even when the pilots find it hard to look at the other plane because of the sun.

3.2 *Modeling Centroid Tracker Performance*

One of the first steps in developing a simulation for the tracker performance is to understand the performance of the individual components. One key component is the speed of the FSM. We measured the amplitude and phase response of the FSM for two different input voltages to confirm the linearity of the device. From this analysis, we observed a distinct phase nonlinearity of the mirror at 74 Hz. This was only apparent when using the stronger 5 V peak to peak signal. Further testing showed that the lower input signal value did not cause this rapid change in phase. Normally one would expect that this sudden change in phase is accompanied by a corresponding overshoot in the magnitude. We simply did not observe this expected increase in gain and have concluded that this effect is a nonlinearity of the FSM. This effect, while not desirable, was deemed not to be a threat to system stability because at 74 Hz, the tracker is operating at a very low gain, making it highly unlikely to generate a signal strong enough to excite the nonlinearity.

From this measurement, the FSM response could be approximated with the transfer function shown in Fig. 5. The Bode plots of the measurements and the transfer function are also shown below to show the quality of the FSM transfer function. It should be noted that the use of third-order system as the fit for a transfer function is unexpected. Normally we would expect that a second-order system would be the correct fit. We opted to use a third-order system because we observed that the magnitude roll-off was greater than 40 dB per decade, and the maximum phase delay was greater than 180 deg. These two observations are the reason for our selection of a third-order system for use in the simulation.

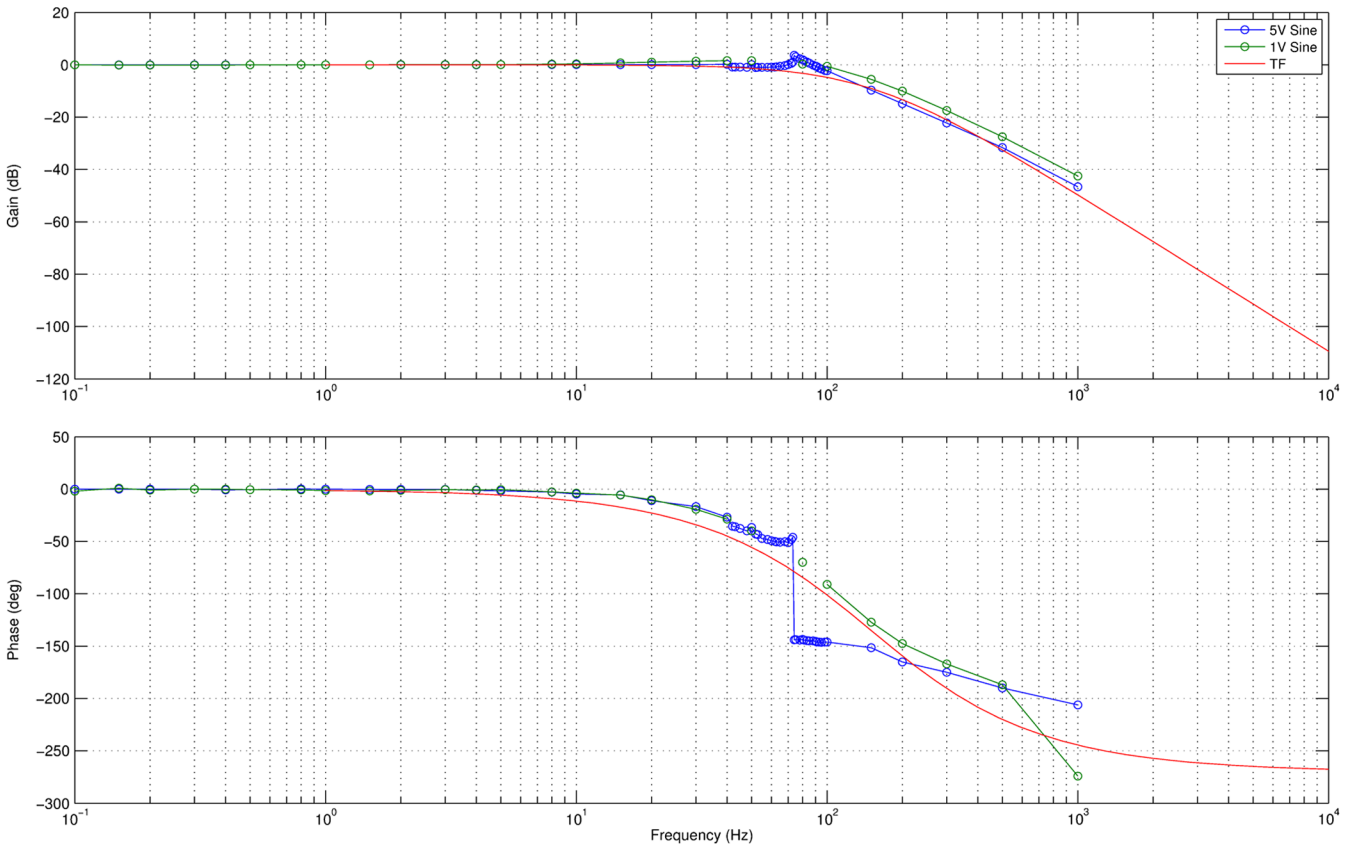

Fig. 5 Measured fast steering mirror (FSM) transfer function compared to function fit.

$$\frac{H_{\mathrm{FSM}}(S)[150^2 * 600 * (2\pi)^3]}{(S + 150 * 2\pi)^2 (S + 600 * 2\pi)}. \quad (2)$$

We were able to treat the rest of the components in the loop as delays. The camera grabbed a frame (with just a few ms of integration time), and that frame was transferred and processed into an error signal. This error signal was then run through a proportional integral differential (PID) controller and sent out the FSM updating the line of sight. This layout was replicated in the Simulink model shown in Fig. 6. It should be noted that there a few gain blocks used to handle the unit conversions between the volts with which the FSM operates and the pixels (which relate to angular tilt) seen by the camera. The disturbance was injected following the FSM representing movement in the line of site. The command into the loop was typically set to zero, as we wanted to measure the ability of the loop to reject disturbances more than to measure the ability of the system to reach a specified command; however, both are related.

The comparison of this model to measure error rejection data shows that that model is an effective means of estimating system performance. We used this model to get a rough set of parameters for the controller and fine-tuned system performance on the hardware. Initial tuning was

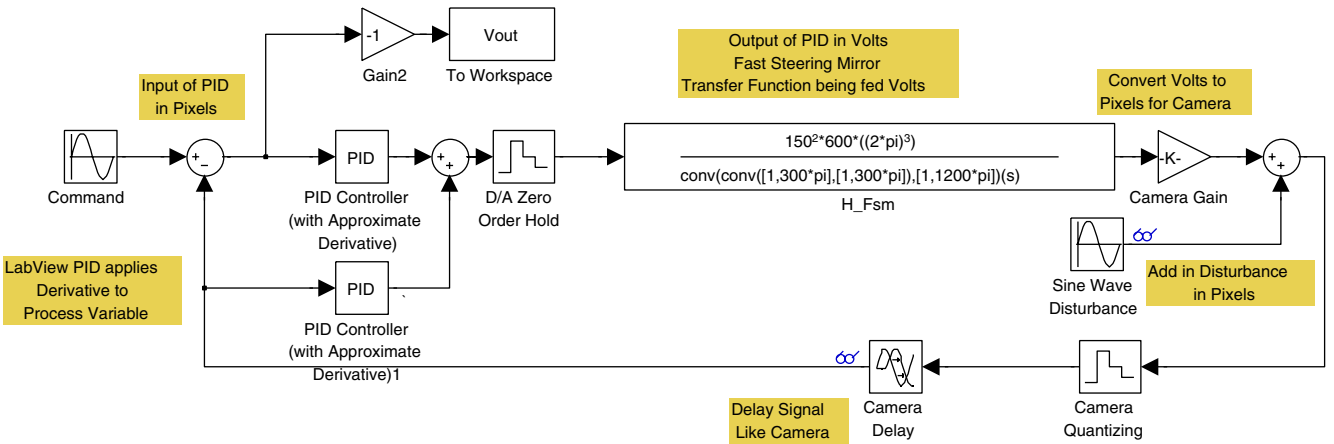

Fig. 6 Simulink™ model of fast steering mirror (FSM) with proportional integral differential (PID) controller.

accomplished using the Zeiger-Nichols method. However, this did not produce satisfactory results. We observed a glitching or jumping of the control signal three to eight times per minute. Most of the time, the jump resolved itself and tracking continued thereafter, but it did make acquisition more difficult. This jump made it difficult to estimate the ultimate gain as the value we arrived at did not include the jump. Further analysis of the jump revealed that a frame from the camera was lost in each case. We investigated a number of methods of eliminating the loss including interrupted driven and polling-type image acquisition loops. We found that with the options exposed by the LabVIEW, controls we were unable to resolve the dropped frames. The missing frame is not known by the centroid tracker. It merely computes the centroid for each frame as soon as it arrives. The effect of the missing frame on the tracker is a periodic increase in latency. This change in latency causes instability after a dropped frame but returns to normal following the drop. We saw no other option but to tune the loop for stability during the max latency of a dropped frame. After detuning the loops, we were able to achieve stable operation to compare to the simulation. The results of this comparison to the less-aggressive tuning are shown in Fig. 7.

From the error rejection transfer function (ERTF) we see a 3-dB point at about 10 Hz, and a crossover at 30 Hz. These values are not particularly good given the frame rate of the camera. Typically the ERTF crossover is at approximately 1/20th the frame rate. For our camera rate, we should have a crossover at 45 Hz. The explanation for the poorer than expected performance is that we had to detune our loop for a latency of two frames, where the 1/20th of the frame-rate estimate is assuming single frame latency.

3.3 *Measured Disturbance Data*

The disturbance data used to generate all of the following simulations was collected from a six-axis accelerometer in the nose of a Cessna Citation 1 during flight. The accelerometer-recorded power spectral densities (PSD) for axial, longitudinal, vertical, tilt, roll, and yaw axes. These data, because they were collected in the nose of the plane, are not completely applicable to our analysis. In the absence of better data, we must assume that PSDs are similar to ones that would be measured at the location of the AAPT install. We see in Fig. 8 an example of typical measured vibrations PSD and back sums. If we multiply the ERTF by the PSD, we will see the modification of the tracker to system performance.

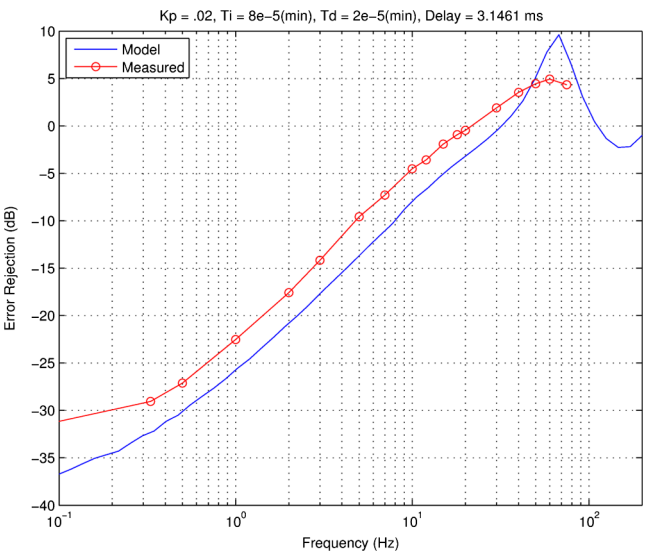

Fig. 7 Tracker performance error rejection transfer function (ERTF) model compared to measurement.

3.4 *Modeling Centroid Tracker Performance*

When we take the ERTF data from Fig. 7 and plot the effect on the PSD from Fig. 8, we get the impact on the back sum of the tracking loop. This result is shown in Fig. 9.

The main observation from this plot is that the tracking loop only has an effect on the low frequencies, but it does reduce the power of the low frequencies by an order of magnitude. This is especially important because those frequencies have the most power. One issue is that there is a lot of power between 10 and 200 Hz. This is a regime that the optical tracker has a limited ability to correct. To improve tracking, we consider a vibration isolation solution.

3.5 *Modeling Centroid Tracker Performance*

The air damper model used for the AAPT system was manufactured by Fabreeka. The model number is PLM 1 and the air dampers have a stiffness of 1714.8 lbm/in, which

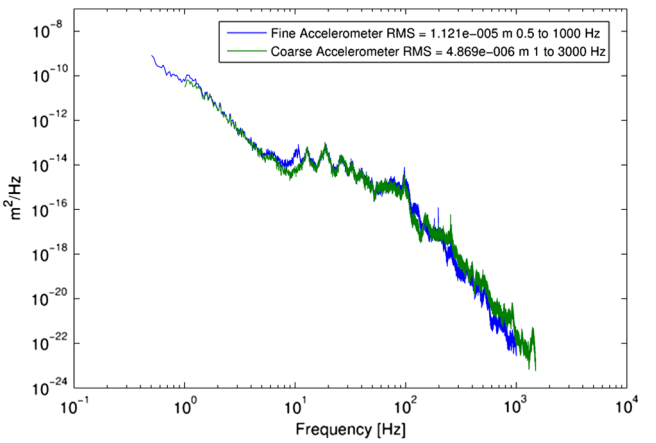

Fig. 8 Typical plot of Boeing's measured vibration represented in power spectral density (PSD). This plot shows the fine and coarse accelerometer data.

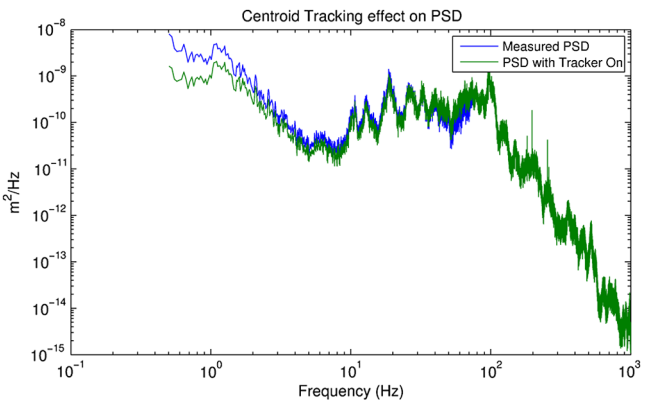

Fig. 9 Effect of closed-loop tracking on vibration power spectral density (PSD).

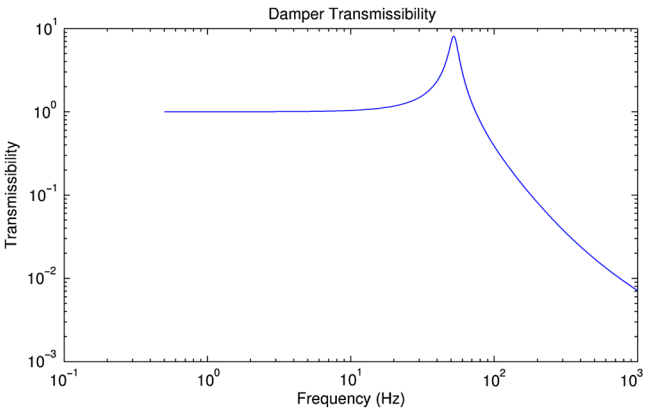

Fig. 10 Transmissibility plot showing two different natural frequency curves, 8 and 55 Hz.

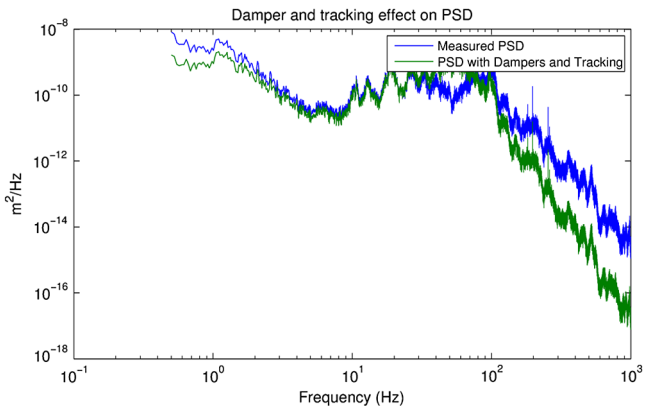

Fig. 11 Power spectral density (PSD) with closed-loop tracking and dampers.

converts to 30,687.187 kg/m. These dampers isolate motion in the z-direction only. The max load for each individual damper is 100 lbs. The AAPT is supported by six of the PLM 1 air dampers, with each of the air dampers inflated between 25 and 35 psi. The air dampers are inflated until the top of the boot is level. Because of uneven weight distribution of the system, the front side boots are inflated to 25 psi and the back side boots, which support more of the structure's weight, are inflated to 35 psi. The transmissibility plot below was calculated using the following equation:

$$T = \frac{\sqrt{1+\zeta^2\left(\frac{\omega}{\omega_n}\right)^2}}{\sqrt{\left[1-\left(\frac{\omega}{\omega_n}\right)^2\right]+4\zeta^2\left(\frac{\omega}{\omega_n}\right)^2}}, \tag{3}$$

where ω is the variable frequency of the system (0–1500 Hz); ω_n is the natural frequency of the air dampers; and $\zeta = C/(2\sqrt{km})$. Also, C is the damping coefficient, and is equal to $m/Q(\sqrt{k/m})$ with m being the mass on the damper, Q being the quality factor, and k being the spring stiffness. The transmissibility of the dampers is shown in Fig. 10.

With accurate loading on the dampers, we compute that the resonant frequency will be ~52 Hz for the dampers. Unfortunately this frequency is also in the frequency band where the centroid tracker also overshoots. Figure 11 shows us the combined performance with the tracker and the dampers installed.

As expected, we see the increase in PSD where the damper response is oscillating (around 52 Hz), but above that frequency, energy is greatly reduced, and in the low frequencies, the tracker is able to improve response. This performance could be further improved by lowering the natural frequency of the dampers and/or improving the error rejection crossover frequency of the tracker.

4 Conclusions

The main purpose for this paper on the AAPT is to detail much of the design process for building an airborne laser tracker. This project was successful because the system constructed was flown successfully in support of the AAOL mission. As of this paper, the AAPT system has been installed and flown for 10 separate test campaigns and logged over 100 h of operating time. The system has demonstrated robustness and has functioned reliably, with the exception of a failed laser. This system is also entirely built using a combination of off-the-shelf components and machined aluminum parts. We feel that the design and construction of this system using only COTS components is a significant accomplishment.

Additionally, for the success of the AAPT project, the AAOL project was also highly successful. Prior to the AAOL flight testing program, available aero-optical data was limited to CFD simulation and wind-tunnel testing. The difficulty in generating this data meant that relatively few data

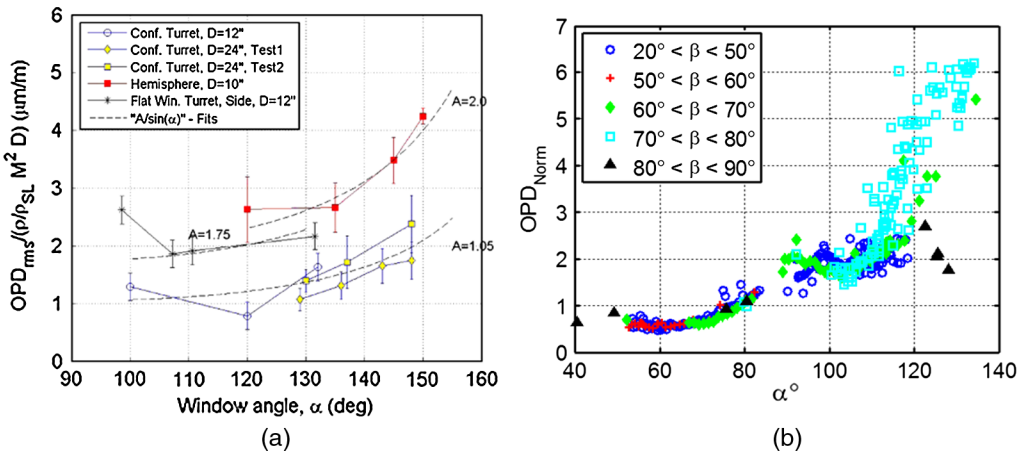

Fig. 12 (a) Available optical path difference (OPD) data as of January 2010;[7] (b) data from a single flight sequence.[8]

points were available. The addition of AAOL flight data means that a much wider variety of look angles are now available to study. Aero-optics is highly spatially varying, and the availability of more angles helps to better understand the phenomenon. The increase in data from AAOL is clearly illustrated in Fig. 12.

In this figure we see that a single week of flight testing provides many times more data than was previously available from all testing. This kind of data availability provides a lot of possibilities for improved knowledge in aero-optical effects. The AAPT project and its success contributed to the greater success of the AAOL project.

Acknowledgments

The views expressed in this paper are those of the authors and do not necessarily reflect the official policy or position of the Air Force, the Department of Defense, or the U.S. Government. These efforts were funded by the HEL-JTO and administered through the Air Force Office for Scientific Research (AFOSR) under Grant No. FA9550-07-1-0574. The U.S. government is authorized to reproduce and distribute reprints for governmental purposes notwithstanding any copyright notation thereon.

References

1. J. Gilbert and L. J. Otten, Eds., "Aero-optical phenomena," in *Progress in Astronautics and Aeronautics*, Vol. 80, AIAA, New York (1982).
2. E. J. Jumper and E. J. Fitzgerald, "Recent advances in aero-optics," *Prog. Aero. Sci.* **37**(3), 299–339 (2001).
3. M. Weng, A. Mani, and S. Gordeyev, "Physics and computation of aero-optics," *Ann. Rev. Fluid Mechan.* **44**, 299–321 (2012).
4. A. E. Smith, S. Gordeyev, and E. J. Jumper, "Recent measurements of aero-optical effects caused by subsonic boundary layers," *Opt. Eng.* **52**(7), 071404 (2012).
5. E. J. Jumper et al., "The Airborne Aero-Optics Laboratory (AAOL)," *Opt. Eng.* **52**(7), 071408 (2013).
6. S. L. Chodos and S. H. Roszkowski, "Image edge location estimate based on the image centroid slope," *Proc. SPIE* **3086**, 200–209 (1997).
7. S. Gordeyev and E. J. Jumper, "Fluid dynamics and aero-optics of turrets," *Prog. Aero. Sci.* **46**(8), 388–400 (2010).
8. C. Porter et al., "Flight measurements of aero-optical distortions from a flat-windowed turret on the airborne aero-optics laboratory (AAOL)," in *42nd AIAA Plasmadynamics and Lasers Conf.*, pp. 27–30 (2011).

Matthew J. Krizo received his BSEE degree from the Cedarville University in 2005. He received his MSEE degree from the University of Dayton, in 2009. He is a research engineer with AFIT's Center for Directed Energy within Engineering Physics department, where he oversees the development and support of the AFIT active pointer/tracker (AAPT).

Salvatore J. Cusumano received the BS and MS degrees in electrical engineering from the U.S. Air Force Academy (1971) and the Air Force Institute of Technology (1977), respectively. He holds a PhD in control theory from the University of Illinois (1988). He currently serves as a senior scientist at MZA, Dayton, Ohio. Prior to his current position at MZA, he taught optics and beam control at the graduate level within the engineering physics department at the Air Force Institute of Technology (AFIT). Originally, he joined AFIT as the director for the Center for Directed Energy at AFIT. Cusumano's research interests are manifest in his 30 years of experience working for the Air Force at Kirtland AFB in directed energy. They include resonator alignment and stabilization, intra-cavity adaptive optics, phased arrays, telescope control, pointing and tracking, adaptive optics, and component technology for directed energy. He holds two patents (jointly) for his work in phased arrays. Cusumano is a member of SPIE, OSA, and DEPS.

Steven T. Fiorino received his BS degrees in geography and meteorology from The Ohio State University (OSU; 1987) and Florida State University (FSU; 1989). He additionally holds an MS in atmospheric dynamics from OSU (1993) and a PhD in physical meteorology from FSU (2002). He is a retired Air Force lieutenant colonel with 21 years of service, and is currently a research associate professor of atmospheric physics within the engineering physics department at AFIT, and the director of the Center for Directed Energy. His research interests include microwave remote sensing, development of weather signal processing algorithms, and atmospheric effects on military systems, such as HEL and weapons of mass destruction. Fiorino is a member of SPIE, AMS, AIAA, and DEPS.

Ryan Heap received his BSME degree from the University of Dayton in 2009. He was a research associate with AFIT's Center for Directed Energy within the engineering physics department when this work was performed, where he led SolidWorks modeling.

Victor Velten received his BSEE degree from the University of Dayton in 2009. He was a research associate with AFIT's Center for Directed Energy within the engineering physics department when this work was performed, where he studied tracking algorithms.

Joshua Brown: Biography not available.

Richard J. Bartell received his BS degree in physics from the U.S. Air Force Academy as a distinguished graduate in 1979. He received his MS degree from the Optical Sciences Center, University of Arizona, in 1987. He was a research physicist with AFIT's Center for Directed Energy within the engineering physics department when this work was performed, where he led development of the HEL end-to-end operational simulation model.